arXiv:1610.06785v1 [cond-mat.mes-hall] 21 Oct 2016

Tailoring non-collinear magnetism by misfit dislocation lines

Aurore Finco,[1] Pin-Jui Hsu,[1] André Kubetzka,[1] Kirsten von Bergmann,[1] and Roland Wiesendanger[1]

[1] *Department of Physics, University of Hamburg, D-20355 Hamburg, Germany*

(Dated: October 24, 2016)

The large epitaxial stress induced by the misfit between a triple atomic layer Fe film and an Ir(111) substrate is relieved by the formation of a dense dislocation line network. Spin-polarized scanning tunneling microscopy (SP-STM) investigations show that the strain is locally varying within the Fe film and that this variation affects the magnetic state of the system. Two types of dislocation line regions can be distinguished and both exhibit spin spirals with strain-dependent periods (ranging from 3 nm to 10 nm). Using a simple micromagnetic model, we attribute the changes of the period of the spin spirals to variations of the effective exchange coupling in the magnetic film. This assumption is supported by the observed dependence of the saturation magnetic field on the spin spiral period. Moreover, magnetic skyrmions appear in an external magnetic field only in one type of dislocation line area, which we impute to the different pinning properties of the dislocation lines.

I. INTRODUCTION

Strain-induced control of complex magnetic states such as spin spirals or skyrmions[1,2] is a multifaceted approach towards manipulation of spin structures. Mechanical or piezoelectrical[3] setups as well as direct influence on the sample growth are used to investigate such effects with multiple experimental techniques on various systems. The observed phenomena are ascribed to changes of the effective anisotropy: uniaxial mechanical compression tunes the stability of the skyrmion lattice phase, e.g. in the helimagnet MnSi[4], where hydrostatic pressure also decreases the helix period and the critical temperature[5]. On the other side, epitaxial strain created by growing multiferroic $BiFeO_3$ thin films on different substrates can destroy the cycloidal spin spiral and stabilize an antiferromagnetic state[6], again via effective anisotropy. The non-collinear magnetic structures mentioned above are stabilized by the Dzyaloshinskii-Moriya interaction (DMI), which can also be affected by strain. This mechanism was found in FeGe, where uniaxial tensile strain dramatically distorts the skyrmion lattice[7].

Although previous studies were mostly focused on the effects of spatially uniform strain, we investigate here the influence of strain variations on a local scale in an ultrathin magnetic film using spin-polarized scanning tunneling microscopy (SP-STM)[8]. Our system consists of three atomic layers of Fe deposited on Ir(111). Because of the misfit between Ir (fcc, lattice constant 3.84 Å) and Fe (bcc, lattice constant 2.86 Å), the triple layer Fe film exhibits a dislocation line network. We observe that the epitaxial strain relief is not uniform within the ultrathin film, resulting in different regions exhibiting spin spirals with various periods and vanishing at different magnetic field intensities. We attribute these differences to spatial variations in the strength of the effective exchange coupling. Depending on the atom arrangement in the magnetic film, these spirals may or may not split up into single magnetic skyrmions[9].

II. EXPERIMENTAL DETAILS

The experiments were performed in a ultrahigh vacuum system with a base pressure below 10^{-11} mbar. Different chambers are used for substrate cleaning, Fe deposition and STM measurements. The Ir single crystal substrate was prepared by cycles of Ar-ion sputtering at 800 eV and annealing up to 1600 K for 60 s. The Fe film was then evaporated onto the clean substrate at elevated temperature (about 200 °C) at a deposition rate around 0.2 atomic layer per minute. Four different scanning tunneling microscopes were used for this work, three low temperature microscopes with He bath cryostats operating at respectively 4 K, 5 K and 8 K as well as a variable temperature system equipped with a He flow cryostat. Out-of-plane external magnetic fields were applied during the low temperature measurements using superconducting coil magnets. We used antiferromagnetic bulk Cr tips for the spin-resolved measurements. All the STM topography images were measured in constant-current mode, where the stabilization current is kept constant by a closed feedback loop. The differential conductance maps were simultaneously recorded at a fixed sample bias voltage using lock-in technique.

III. MORPHOLOGY OF THE FE FILM

The STM topography map presented in Fig. 1(a) shows a typical triple layer Fe film on an Ir(111) substrate. The surface of the film exhibits a dense network of dislocation lines. These lines follow the three equivalent high-symmetry directions $\langle 11\bar{2}\rangle$ of the fcc(111) surface[9] as already reported for the double layer Fe film[10].

Two types of dislocation lines can be distinguished from the STM image of Fig. 1(a): at positive sample bias voltage, the dislocation lines in the region spanned by the white dashed arrow show an alternating bright and dark contrast as well as double line features (see detail in Fig. 1(b)). These areas will thus be named *double lines* in the following. The spacing for double lines is

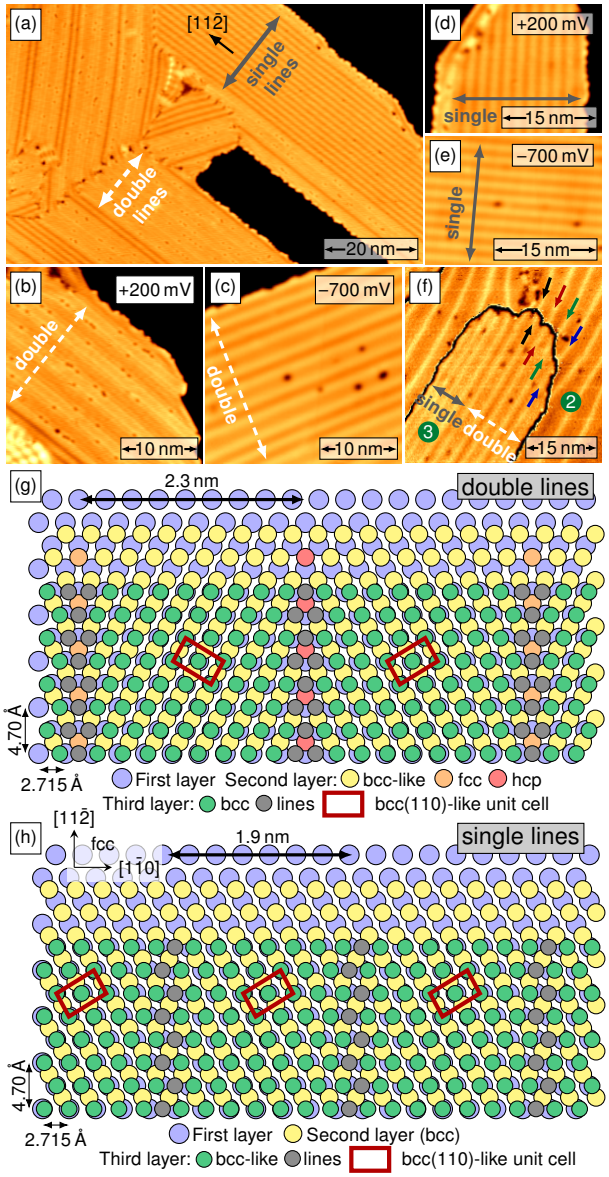

FIG. 1. (a) Constant-current STM topography map of the triple layer Fe film on Ir(111). Double and single lines are indicated by the arrows. (b),(c) Zoom-in on double line areas. At positive bias, one can see that bright and dark lines alternate and show a double line feature, whereas at negative bias, the lines look all very similar. (d),(e) STM topography of single line regions. The single lines have the same appearance at any sample bias voltage. (f) Constant-current STM topography map of a triple layer Fe island on top of a double layer Fe film. The numbers in green circles indicate the local thickness of the film. The color scale was adjusted separately for the two terraces in order to highlight the matching of the dislocation lines. The areas between the bright lines on the double layer are bcc. (g),(h) Proposed structure models for the triple layer Fe film from the experimental observations presented in (a)-(f). *Measurement parameters:* $I = 1\,\mathrm{nA}$ and (a) $U = +200\,\mathrm{mV}$, $T = 8\,\mathrm{K}$, $B = 3.5\,\mathrm{T}$; (b) $T = 5\,\mathrm{K}$, $B = 4.5\,\mathrm{T}$; (c) $T = 5\,\mathrm{K}$, $B = 3\,\mathrm{T}$; (d) $T = 8\,\mathrm{K}$, $B = 0\,\mathrm{T}$; (e) $T = 8\,\mathrm{K}$, $B = 2.5\,\mathrm{T}$; (f) $U = -700\,\mathrm{mV}$, $T = 153\,\mathrm{K}$, $B = 3\,\mathrm{T}$.

ranging from 2.3 nm to 3 nm, which corresponds to half the structural period. On the other hand, in the region marked by the gray arrow, the lines are denser (spacing between 1.8 nm and 2.2 nm) and they all have the same appearance at any bias voltage (see Fig. 1(d) and Fig. 1(e)). Hence these lines will be designated as *single lines*. At negative sample bias voltage, the distinction between single and double lines from the sole topography becomes challenging as illustrated in Fig. 1(c) and Fig. 1(e).

Figures 1(g) and 1(h) show proposed atomic structure models for the triple layer Fe film. In both cases, the first layer Fe is pseudomorphic with respect to the Ir(111) substrate lattice[11]. The double lines are located exactly on top of the dislocation lines of the double layer Fe film as shown in Fig. 1(f). The double layer lines seem to get closer when they approach the island: the strain relief is larger in the triple than in the double layer. In the atomic model, the second layer is uniaxially compressed with respect to a pseudomorphic layer and the arrangement of the Fe atoms is getting close to bcc(110). The lines correspond to the positions where the atoms are located on the fcc or hcp sites and the triple layer follows a bcc stacking on top of the double layer. In the case of the single lines, also the second layer grows pseudomorphically but in bcc stacking (see Fig. 1(h)) and only the third layer on top is uniaxially compressed. All the lines are identical and induced by lateral shifts of the atoms. As will be shown later by looking at the magnetic structure, the double line regions have mirror planes along the dislocation lines, whereas two mirror symmetric domains exist for the single line regions, in agreement with the structure model.

IV. ZERO FIELD NON-COLLINEAR MAGNETIC STRUCTURE

The difference between single and double line areas becomes more striking when we look at the magnetic structure. Figures 2(a) and 2(b) show respectively a spin-resolved constant-current map and a simultaneously spin-resolved differential conductance map measured with an out-of-plane spin-sensitive Cr bulk tip at low temperature. These SP-STM measurements reveal that spin spirals propagate along both types of dislocation lines. The nature of the spin spirals is cycloidal: this has been shown already for the double layer Fe spirals[10] as well as for the double line regions in the triple layer Fe[9] and is assumed also to be the case for the single line areas since the Fe-Ir interface-induced DMI is large[11]. However, the appearance of the spin spirals varies in the different regions of the Fe film. The wavelength of the spirals is smaller in the double line regions (3 nm to 4.5 nm) than in the single line regions (between 5 nm and 10 nm).

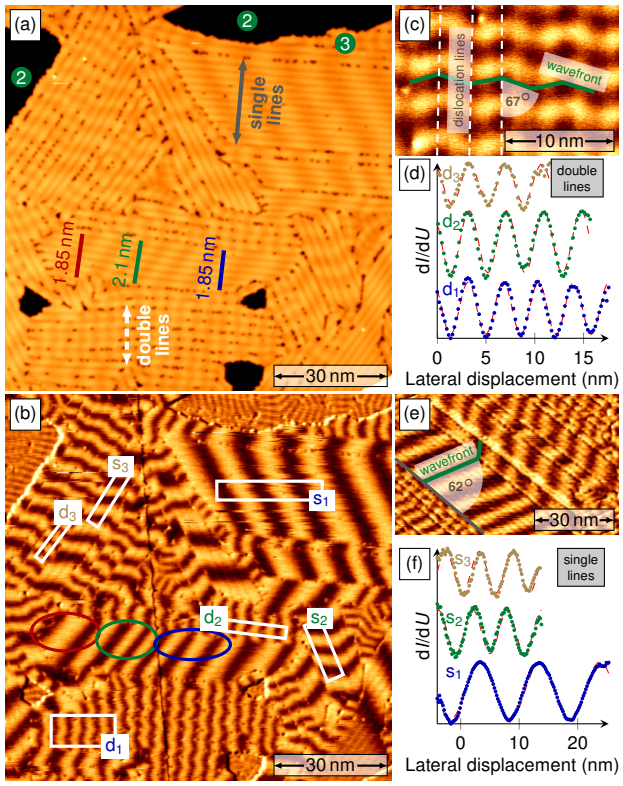

FIG. 2. (a),(b) Spin-resolved constant-current map and spin-resolved differential tunneling conductance map of a triple layer Fe film on Ir(111) measured simultaneously using a Cr bulk tip with out-of-plane spin sensitivity. The magnetic sensitivity of the tip is simply deduced from the magnetic contrast on the spirals, which is identical for all the propagation directions. The magnetic contrast is visible on both the constant-current and differential conductance maps. The ellipses on image (b) mark a zone where the period of the spiral is changing: this can be correlated with the spacing between the dislocation lines indicated in (a). (c) Detail of the spin-resolved differential tunneling conductance map of a double line region. The spin spiral propagates along the lines and its wavefront exhibits a zigzag shape. (d),(f) Line profiles taken in the double and single line regions, respectively, at the positions indicated in (b). The displayed profiles are the mean values within the rectangles, each data line was laterally shifted to straighten the wavefront and offsets were applied to the resulting profiles for clarity. The red dashed lines are the results of fits with sine functions, showing that the spirals are homogeneous regardless of the considered region. (e) Spin-resolved differential conductance map of an area with single lines. Spin spirals with various wavelengths are visible and their wavefronts are tilted by about $\pm 62°$ with respect to the lines. *Measurement parameters:* no external magnetic field, (a),(b) $U = -700\,\mathrm{mV}$, $I = 1\,\mathrm{nA}$, $T = 8\,\mathrm{K}$; (c) $U = -700\,\mathrm{mV}$, $I = 750\,\mathrm{pA}$, $T = 4\,\mathrm{K}$; (e) $U = -700\,\mathrm{mV}$, $I = 1\,\mathrm{nA}$, $T = 8\,\mathrm{K}$.

Furthermore, the wavefront of the double line spirals has a zigzag shape[9,10], whereas that of the spirals in the single line regions is straight but tilted with respect to the lines as can be seen from the details of spin-resolved differential conductance maps in Fig. 2(c) and Fig. 2(e). The proposed structure models can explain these shapes for the wavefronts: the wavevector prefers to follow the bcc[001]-like rows of atoms as observed for the double layer Fe on Ir(111)[10], Cu(111)[12] and W(110)[13]. For the double lines, the direction of the rows alternate and this creates the magnetic zigzag structure, whereas the direction does not change for the single lines, as shown by the bcc(110)-like unit cells marked in red in Fig. 1(g) and Fig. 1(h). However, for the single line regions, two mirror symmetric structural domains are possible and found in the SP-STM data.

For a strict coupling of the wavevector to the bcc [001] direction, the expected angle α between the wavefront and the dislocation lines (as defined in Fig. 2(c) and Fig. 2(e)) can be computed from the structure models:

$$\tan\alpha = \frac{\sqrt{3}\delta}{\delta + a} \qquad (1)$$

where δ is the line spacing and $a = 2.715\,\text{Å}$ the in-plane interatomic distance for Ir(111). This expression is the same for both structures. This angle is below 60° and decreases with the line spacing. Yet the angle obtained from the data is slightly larger (up to 10°) and seems to change randomly. This deviation which is going towards a straighter wavefront for the double line regions was previously observed for the double layer spirals[10]. The guiding of the wavevector might compete here with the presence of energetically disadvantageous kinks in the wavefront. For the single line areas, the angle is also larger, meaning that the wavefront is more perpendicular to the dislocation lines than expected. This effect could be attributed to boundary effects as well as to domain wall-like structures preferring to be as short as possible. Line profiles of spirals (Fig. 2(d) and Fig. 2(f)) taken in various regions can be fitted with sine functions. This sinusoidal shape indicates that the spirals are homogeneous, i.e. no direction of the magnetic moments is more favorable than the others. Yet epitaxial strain in ultrathin films creates an effective anisotropy via magnetoelastic coupling[14] and since the strain relief is not uniform in the triple layer Fe film, the total effective magnetic anisotropy is expected to vary between the different regions. This should result in more or less pronounced distortions of the spiral profiles depending on the dislocation line spacing. We therefore conclude from the homogeneity of all the observed spiral profiles that the effective magnetic anisotropy and its variations in the triple layer Fe film are small enough to be neglected in the following.

V. TUNING OF THE SPIRAL PERIOD WITH STRAIN RELIEF

In Fig. 2(b), a single line area in which the wavelength of the spiral is changing is marked with ellipses. This variation occurs because the dislocation lines become more distant in the green zone than in the surrounding red and blue ones. The distance between the lines in each ellipse is given in the constant-current map of Fig. 2(a).

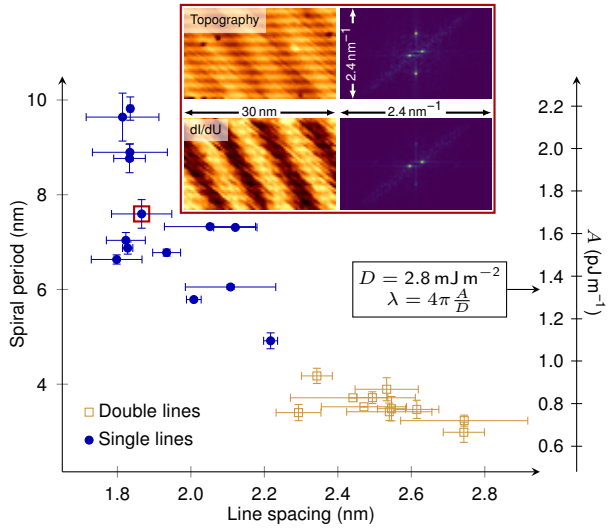

FIG. 3. Dependence of the spiral period on the spacing of the dislocation lines for the triple layer Fe on Ir(111), both double and single line regions. The SP-STM measurements were performed at low temperature (4 K or 8 K) on several different samples and the spiral periods were extracted using 2D Fourier transformation and fits of the real space data to sine functions, keeping only points with an error bar below 15%. For the double line regions, the zigzag shape of the wavefront was not considered and the period was measured along the lines. The actual wavelength along the direction of the wavevector might be 10% smaller. On the single line regions, the angle of the wavefront was taken into account in the determination of the period. It is evident that if the distance between the dislocation lines decreases, the spiral period increases, as observed already in Fig. 2. The insets show the data (both spin-resolved constant-current map and differential conductance map as well as their Fourier transforms) used to determine the point marked with the red square. The axis on the right indicates that the effective exchange parameter should vary between 0.6 pJ m^{-1} and 2.2 pJ m^{-1} to create spirals with wavelengths between 3 nm and 10 nm from the simple model described in the text.

The closer the lines, i.e. the larger the compression in the third layer Fe, the larger the spiral period.

The graph in Fig. 3 presents a systematic investigation of the effect of the strain relief on the wavelength of the spirals, for both double and single line regions. The spiral period and the spacing between dislocation lines were measured using Fourier transforms and fits of the real space data to sine functions in several different regions on several samples. The trend observed in Fig. 2 is confirmed, the spiral period decreases when the line spacing increases. The line spacing is linked to the amplitude of the strain relief by the structure models: the mean value of the distance between the Fe atoms in the fcc [1$\bar{1}$0] direction in the top layer decreases with the line spacing. To give an order of magnitude, this distance is 5% smaller for a 1.8 nm than for a 3 nm line spacing.

When the distance between the dislocation lines changes, all the interatomic distances in the Fe film are modified, thus it is expected that the strengths of the magnetic interactions will be affected. The relevant interactions for this system are the exchange couplings and the interface-induced DMI[1,15]. Based on the data shown in Fig. 2(d) and Fig. 2(f), we assume that the effective anisotropy is negligible. The DMI originates mainly from the Fe-Ir interface and since the first layer Fe layer is pseudomorphic regardless of the considered region, it should not be significantly influenced (contrary to bulk systems like FeGe[7]). We therefore infer that the strain relief is acting mostly on the exchange couplings to modify the period of the spirals.

Ab initio calculations for a free-standing Fe bcc(110) layer[16] also assigned the period variation of the spirals as well as their stability under in-plane strain to modifications of the exchange couplings. However, the spin spiral state is only stable in the free layer when a compressive strain is applied and the compression reduces the period of the spiral. The calculated evolution of the spirals with the strain is thus opposite to what we measured but this discrepancy could result from the presence of the substrate and the complicated atomic structure of the Fe film.

In order to estimate the magnitude of the strain effect, we consider a simplified one-dimensional micromagnetic model derived from the one proposed by Bogdanov and Hubert[17] in which only the effective isotropic exchange coupling and the DMI are kept. We completely ignore here that the film is not spatially uniform, resulting in spatially inhomogeneous magnetic coupling constants. Only average values are taken into account. The energy density is thus:

$$\mathcal{E} = A\sum_i \left(\frac{\partial \mathbf{m}}{\partial x_i}\right)^2 + D\left(\mathrm{m}_z\frac{\partial \mathrm{m}_x}{\partial x} - \mathrm{m}_x\frac{\partial \mathrm{m}_z}{\partial x}\right) \qquad (2)$$

where A is the effective exchange stiffness constant, D the effective DMI constant and $\mathbf{m}$ the reduced dimensionless magnetization. In this particular case, there is always a stable cycloidal spin spiral state in the system and its period λ is simply:

$$\lambda = 4\pi\frac{A}{D} \qquad (3)$$

For the monolayer Fe on Ir(111), the value of the DMI constant from *ab initio* calculations is $|d| = 1.8\,\mathrm{meV}$ [11] which gives the micromagnetic parameter $D = 2.8\,\mathrm{mJ\,m^{-2}}$ for a three-layer-thick Fe film. As shown in Fig. 3, the exchange stiffness parameter should then vary between 0.6 pJ m^{-1} and 2.2 pJ m^{-1} to obtain magnetic periods ranging from 3 nm to 10 nm. These values are similar to $A = 2.0\,\mathrm{pJ\,m^{-1}}$ found for the PdFe bilayer on Ir(111) [18] with a spiral period of about 6 nm. Since the DMI originates from the interface, its effect should decrease when the thickness of the film increases, i.e. the typical length scale of the magnetic structure is expected to become larger. Indeed, the period of the nanoskyrmion lattice on the monolayer Fe on Ir(111) is

1 nm[11], the wavelength of the double layer spiral is about 1.6 nm[10] and for patches of a size below 100 nm (larger ones were not found on the samples), the quadruple layer appears ferromagnetic (as, for example, in Fig. 5).

VI. SKYRMIONS AND DOMAIN WALLS IN MAGNETIC FIELD

In external out-of-plane magnetic fields between 1 T and 3 T, the spin spirals in the double line regions split up into distorted magnetic skyrmions[9], as illustrated in Fig. 4. In contrast, no skyrmion is created on the single line regions. There, the spirals become inhomogeneous and behave like an assembly of independent 360° domain walls which disappear one by one when the field is increased. Adding a Zeeman term to the model proposed before (equation (2)) does not allow to understand this difference. For a isotropic film without effective anisotropy, there is a stable skyrmionic phase for any couple (A, D) under the appropriate external magnetic field. The crucial point for the triple layer Fe film on Ir(111) are the dislocation lines which break the rotational symmetry. Thus one cannot expect the existence of the typical circular shaped skyrmions[19] as observed, for example, in the PdFe bilayer on Ir(111)[20] and a priori, even the presence of skyrmions is not obvious. Nevertheless, distorted skyrmions appear in the double line regions. Their bean-like shape is induced by the local arrangement of the Fe atoms similarly to the zigzag shape of the spin spiral wavefront. They are always located on top of three dislocation lines, two identical ones at the ends and a third different one in the center. This particular preferred position results from the local variation of the magnetic interaction within the layer. The skyrmions are hence pinned to the lines and naturally aligned on "tracks" (see Fig. 4 and Fig. 5(g)). The atom arrangement is different for the single lines and it appears that the skyrmion pinning effect is absent and only 360° domain walls are observed in magnetic field.

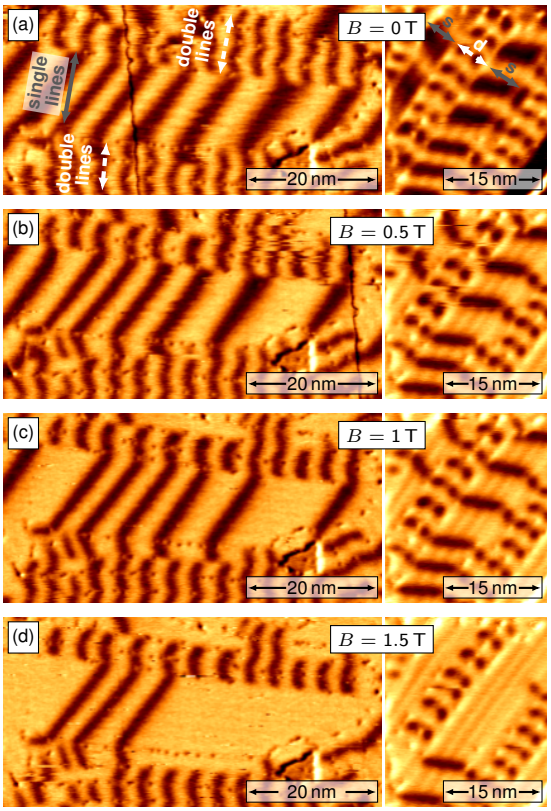

FIG. 4. Spin-resolved differential tunneling conductance maps of a region with single lines surrounded by double lines (left) and of a region with double lines surrounded by single lines (right) in increasing out-of-plane magnetic field, measured with an out-of-plane spin-sensitive Cr bulk tip. When the external field increases, the spin spirals in the double line regions transform into distorted skyrmions whereas those in the areas with single lines become inhomogeneous and can be described as an assembly of independent 360° domain walls. When the width of these walls is similar to the width of the skyrmions in the adjacent areas, they couple to them. *Measurement parameters:* Left: $U = -700$ mV, $I = 1$ nA, $T = 8$ K; Right: $U = -500$ mV, $I = 1$ nA, $T = 4$ K.

VII. METASTABILITY AND TRANSITION FIELDS

A more quantitative investigation of the influence of an external magnetic field is shown in Fig. 5. For this measurement series, the magnetic field was increased up to 4 T in 0.5 T steps. At 4 T, the sample has fully reached the ferromagnetic state. Then, the magnetic field was decreased again in steps to zero. Every region in the film behaves differently because of its structure and its interactions with adjacent areas (see Fig. 4). Comparisons between pictures taken at the same field value during the up-sweep and the down-sweep reveal, however, that almost all the areas show hysteresis. The skyrmions and domain walls vanish at a much higher field than the one needed to produce them again. This indicates that the magnetic states are metastable.

The transition fields to the ferromagnetic (FM) state are obtained from field dependent measurements using the procedure described in Fig. 5(i): the evolution of the magnetic states for different regions is indicated for an up- and a down-sweep of the magnetic field. The transition field value corresponds to the middle of the corresponding step and the error bar to the step height.

Results for several samples are gathered in Fig. 6, where they are correlated with the spiral period in the absence of external magnetic field. Only sweeps with increasing field are considered in this figure, the field values are thus upper estimates due to the hysteresis effect. The transition field B_t is decreasing when the spiral period increases. The trend that higher external fields are required to destroy non-collinear spin structures with smaller spatial period is consistent which the observation that the

FIG. 5. (a)-(h) Spin-polarized differential tunneling conductance maps of an ultrathin Fe film on Ir(111). The numbers in green circles in (a) indicate the local Fe coverage. An external out-of-plane magnetic field was applied, increased in steps of 0.5 T up to 4 T (at this field the sample is completely polarized, i.e. ferromagnetic) and then decreased again to zero. Comparison between scans taken at the same field value shows a hysteretic behavior for the triple layer Fe, both in the regions with the double and single lines. (i) Plot of the magnetic state during the field sweep of the four areas marked in blue in (a). Areas I and II are double line regions, III and IV single line regions. *Measurement parameters:* $U = -500\,\mathrm{mV}, I = 1\,\mathrm{nA}, T = 4\,\mathrm{K}$, out-of-plane spin-sensitive Cr bulk tip.

spin spiral in the double layer Fe does not change in magnetic fields up to 9 T[10].

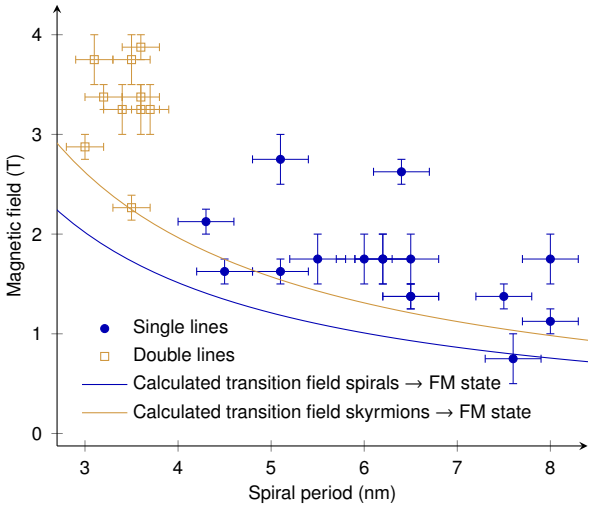
Magnetic field (T)
Spiral period (nm)
Single lines
Double lines
Calculated transition field spirals → FM state
Calculated transition field skyrmions → FM state

FIG. 6. Effect of the spiral period on the magnetic fields needed to reach the ferromagnetic state during an increasing field sweep. The correlation between the spiral period and spacing of the dislocation lines in the Fe layer shown in Fig. 3 leads also to a dependence of the transition field on the strain relief. A trend that higher external fields are required to destroy non-collinear spin structures with smaller spatial period appears. The calculated transition fields were obtained from the phase diagram detailed by Bogdanov and Hubert[17] with the parameters from Fig. 3: $D = 2.8\,\mathrm{mJ\,m^{-2}}$ and $K_{\mathrm{eff}} = 0$. The magnetic moment used is $\mu = 2.7\mu_{\mathrm{B}}$ per Fe atom[11]. Because of the metastability of the magnetic states revealed by the hysteresis, the experimental field values are upper estimates of the transition fields. The SP-STM measurements were performed at 4 K on three different samples and the external magnetic field was increased in steps of 0.5 T. The error bars correspond to the height of the steps as indicated in Fig. 5(i).

Although the simplified model (2) does not help to understand the absence of a skyrmionic phase in the single line regions, it reproduces the decrease of the transition field for larger magnetic structures once the Zeeman term $\mathcal{E}_{\mathrm{z}} = -M_{\mathrm{s}} B \mathrm{m}_z$ is included. In the zero effective anisotropy case, the transition field can be obtained from the phase diagram provided by Bogdanov and Hubert[17]. There is a threshold value for the reduced field parameter h such as:

$$B_{\mathrm{t}} = \frac{D^2 h_{\mathrm{t}}}{A M_{\mathrm{s}}} = 4\pi \frac{D h_{\mathrm{t}}}{\lambda M_{\mathrm{s}}} \tag{4}$$

The saturation magnetization $M_{\mathrm{s}} = 1.77\,\mathrm{MA\,m^{-1}}$ is estimated from the magnetic moment of 2.7 μ_{B} per atom in the monolayer Fe[11]. We did not consider here a potential variation of M_{s} with the strain relief. The threshold value h_{t} is different for the transition from spirals to the

FM state and from skyrmions to the FM state:

$$h_{\mathrm{t}}^{\mathrm{spiral}} = 0.308 \quad (5)$$

$$h_{\mathrm{t}}^{\mathrm{skyrmion}} = 0.401 \quad (6)$$

The transition fields are plotted as plain lines in Fig. 6, assuming again that $D = 2.8\,\mathrm{mJ\,m^{-2}}$. They are defined as the fields at which the energy of the FM state is equal to the one of the spiral or skyrmion state, respectively. As expected, the experimental values are larger than the computed ones because of the metastability of the spiral and skyrmion states in increasing magnetic field. Remarkably, the smallest field values are almost on the theoretical curve and none of them below, which indicates a rather good agreement between the model and the actual system. This behavior of the transition fields supports our assumption that the effective exchange coupling is affected by the strain relief and is responsible for the observed variation of the magnetic properties of the Fe film.

VIII. CONCLUSION

Exploiting the strain relief in epitaxial ultrathin films is an effective way to control precisely and locally their magnetic state. Both the typical size of the spin structures and the transition fields could be tuned. Moreover, the actual uniaxial structure and pinning properties of ultrathin films exhibiting dislocation lines may allow to stabilize a skyrmion state as well as to confine skyrmions on well-defined tracks on the order of a few nanometers. Combined with the possibility to write and delete the skyrmions by a local electric field[9], this could be of great interest in view of future racetrack-based spintronic devices[21–23].

ACKNOWLEDGMENTS

Financial support by the European Union via the Horizon 2020 research and innovation programme under grant agreement No. 665095, by the Deutsche Forschungsgemeinschaft via SFB668-A8, and by the Hamburgische Stiftung für Wissenschaften, Entwicklung und Kultur Helmut und Hannelore Greve is gratefully acknowledged.

[1] K. von Bergmann, A. Kubetzka, O. Pietzsch, and R. Wiesendanger, Journal of Physics: Condensed Matter **26**, 394002 (2014).
[2] N. Nagaosa and Y. Tokura, Nature Nanotechnology **8**, 899 (2013).
[3] J. Cui, J. L. Hockel, P. K. Nordeen, D. M. Pisani, C.-y. Liang, G. P. Carman, and C. S. Lynch, Applied Physics Letters **103**, 232905 (2013).
[4] Y. Nii, T. Nakajima, A. Kikkawa, Y. Yamasaki, K. Ohishi, J. Suzuki, Y. Taguchi, T. Arima, Y. Tokura, and Y. Iwasa, Nature Communications **6**, 8539 (2015).
[5] B. Fåk, R. A. Sadykov, J. Flouquet, and G. Lapertot, Journal of Physics: Condensed Matter **17**, 1635 (2005).
[6] D. Sando, A. Agbelele, D. Rahmedov, J. Liu, P. Rovillain, C. Toulouse, I. C. Infante, A. P. Pyatakov, S. Fusil, E. Jacquet, C. Carrtro, C. Deranlot, S. Lisenkov, D. Wang, J.-M. Le Breton, M. Cazayous, A. Sacuto, J. Juraszek, A. K. Zvezdin, L. Bellaiche, B. Dkhil, A. Barthélémy, and M. Bibes, Nature Materials **12**, 641 (2013).
[7] K. Shibata, J. Iwasaki, N. Kanazawa, S. Aizawa, T. Tanigaki, M. Shirai, T. Nakajima, M. Kubota, M. Kawasaki, H. S. Park, D. Shindo, N. Nagaosa, and Y. Tokura, Nature Nanotechnology **10**, 589 (2015).
[8] R. Wiesendanger, Reviews of Modern Physics **81**, 1495 (2009).
[9] P.-J. Hsu, A. Kubetzka, A. Finco, N. Romming, K. von Bergmann, and R. Wiesendanger, Nature Nanotechnology In press.
[10] P.-J. Hsu, A. Finco, L. Schmidt, A. Kubetzka, K. von Bergmann, and R. Wiesendanger, Physical Review Letters **116**, 017201 (2016).
[11] S. Heinze, K. von Bergmann, M. Menzel, J. Brede, A. Kubetzka, R. Wiesendanger, G. Bihlmayer, and S. Blügel, Nature Physics **7**, 713 (2011).
[12] S.-H. Phark, J. A. Fischer, M. Corbetta, D. Sander, K. Nakamura, and J. Kirschner, Nature Communications **5** (2014).
[13] S. Meckler, N. Mikuszeit, A. Preßler, E. Y. Vedmedenko, O. Pietzsch, and R. Wiesendanger, Physical Review Letters **103**, 157201 (2009).
[14] P. Bruno and J.-P. Renard, Applied Physics A **49**, 499 (1989).
[15] A. Fert and P. M. Levy, Physical Review Letters **44**, 1538 (1980).
[16] T. Shimada, J. Okuno, and T. Kitamura, Physical Review B **85** (2012).
[17] A. Bogdanov and A. Hubert, Journal of Magnetism and Magnetic Materials **138**, 255 (1994).
[18] N. Romming, A. Kubetzka, C. Hanneken, K. von Bergmann, and R. Wiesendanger, Physical Review Letters **114**, 177203 (2015).
[19] J. Hagemeister, E. Y. Vedmedenko, and R. Wiesendanger, Physical Review B **94**, 104434 (2016).
[20] N. Romming, C. Hanneken, M. Menzel, J. E. Bickel, B. Wolter, K. von Bergmann, A. Kubetzka, and R. Wiesendanger, Science **341**, 636 (2013).
[21] S. S. P. Parkin, M. Hayashi, and L. Thomas, Science **320**, 190 (2008).
[22] A. Fert, V. Cros, and J. Sampaio, Nature Nanotechnology **8**, 152 (2013).
[23] R. Wiesendanger, Nature Reviews Materials **1**, 16044 (2016).